Loss of Prohibitin Induces Mitochondrial Damages Altering β-Cell Function and Survival and Is Responsible for Gradual Diabetes Development

Sachin Supale,[1] Fabrizio Thorel,[2] Carsten Merkwirth,[3] Asllan Gjinovci,[1] Pedro L. Herrera,[2] Luca Scorrano,[1] Paolo Meda,[1] Thomas Langer,[3] and Pierre Maechler[1]

Prohibitins are highly conserved proteins mainly implicated in the maintenance of mitochondrial function and architecture. Their dysfunctions are associated with aging, cancer, obesity, and inflammation. However, their possible role in pancreatic β-cells remains unknown. The current study documents the expression of prohibitins in human and rodent islets and their key role for β-cell function and survival. Ablation of *Phb2* in mouse β-cells sequentially resulted in impairment of mitochondrial function and insulin secretion, loss of β-cells, progressive alteration of glucose homeostasis, and, ultimately, severe diabetes. Remarkably, these events progressed over a 3-week period of time after weaning. Defective insulin supply in β-*Phb2*$^{-/-}$ mice was contributed by both β-cell dysfunction and apoptosis, temporarily compensated by increased β-cell proliferation. At the molecular level, we observed that deletion of Phb2 caused mitochondrial abnormalities, including reduction of mitochondrial DNA copy number and respiratory chain complex IV levels, altered mitochondrial activity, cleavage of L-optic atrophy 1, and mitochondrial fragmentation. Overall, our data demonstrate that Phb2 is essential for metabolic activation of mitochondria and, as a consequence, for function and survival of β-cells. ***Diabetes*** **62:3488–3499, 2013**

Canonical glucose-stimulated insulin secretion (GSIS) involves three main components associated with mitochondria (1). First, upstream of mitochondria, glucose enters the cell and is phosphorylated by glucokinase, initiating glycolysis to generate pyruvate. Second, mitochondrial metabolism of pyruvate leads to the generation of ATP along with metabolic coupling factors. Finally, downstream of mitochondrial activation, ATP closes K_{ATP} channels, thereby promoting plasma membrane depolarization inducing elevation of cytosolic Ca^{2+} and insulin exocytosis. Lack of insulin secretory response to glucose by mitochondrial DNA (mtDNA) depleted β-cells provided compelling evidence that mitochondrial activation is not dispensable in metabolism-secretion coupling (2). Likewise, β-cell–specific ablation of mitochondrial transcription factor Tfam results in mtDNA loss, mitochondrial dysfunction, and diabetes in mice (3). To date, several mitochondrial defects have been associated with β-cell dysfunction, including oxidative stress, nutrient toxicity, or altered mitochondrial morphology (4).

β-Cell mitochondria are interconnected and dynamic (5–7). Functional and morphological impairments of β-cell mitochondria have been associated with insulin secretory defects in type 2 patients with diabetes (8). In addition, animal models of diabetes have shown altered mitochondrial morphology, suggesting possible implication of mitochondrial dynamics in maintaining β-cell function (4). This was studied in vitro (6,7) and recently documented in vivo after deletion of the mitochondrial fusion protein optic atrophy 1 (Opa1) in β-cells, leading to defective mitochondrial activation and GSIS, which made mice hyperglycemic (9).

Prohibitins are evolutionary highly conserved proteins that are ubiquitously expressed in eukaryotic organisms, mostly in tissues with high mitochondrial metabolism (10). These proteins have been implicated in pleiotropic functions, such as cell-cycle progression, transcriptional regulation, cell signaling, apoptosis, and mitochondrial biogenesis (11–13). Prohibitins have also been associated with pathological conditions such as inflammation, obesity, and cancer (11,14,15). The prohibitin family comprises two functionally and physically interdependent homologs, Prohibitin-1 (Phb1) and Prohibitin-2 (Phb2), forming heterodimers assembled in ring-shaped complexes within the mitochondrial inner membrane (16). These complexes have been proposed to serve as molecular scaffolds maintaining the integrity of the mitochondrial inner membrane (16). Silencing of *Phb1* in endothelial cells reduces mitochondrial membrane potential and complex I activity (17). Moreover, deletion of *Phb2* in mouse embryonic fibroblasts impairs their proliferation and alters mitochondrial morphology (18). These effects have been mainly attributed to excessive proteolysis of Opa1 long isoforms secondary to Phb2 loss (18).

In order to investigate the role of Phb2 in an endocrine cell type, we have generated β-cell–specific *Phb2* knockout mice. Our results demonstrate that loss of Phb2 caused accelerated proteolysis of Opa1, associated with altered mitochondrial network and function. Furthermore, we observed lower mtDNA copy number and reduced complex IV levels. These events led to β-cell dysfunction and a concomitant β-cell loss, which induced severe diabetes in these animals.

RESEARCH DESIGN AND METHODS

Generation of β-cell–specific *Phb2* knockout mice. *Phb2*$^{fl/fl}$ (18) and Rip*Cre* mice (19) were crossed to generate *Phb2*$^{fl/fl}$, Rip*Cre*$^{+}$ mice designated as β-*Phb2*$^{-/-}$. In order to maintain single copy of the Rip*Cre* allele in

From the [1]Department of Cell Physiology and Metabolism, University of Geneva Medical Centre, Geneva, Switzerland; the [2]Department of Genetic Medicine and Development, University of Geneva Medical Centre, Geneva, Switzerland; and the [3]Institute for Genetics, University of Cologne, Cologne, Germany.

Corresponding author: Pierre Maechler, pierre.maechler@unige.ch.

Received 29 January 2013 and accepted 4 July 2013.

DOI: 10.2337/db13-0152

This article contains Supplementary Data online at http://diabetes.diabetesjournals.org/lookup/suppl/doi:10.2337/db13-0152/-/DC1.

C.M. is currently affiliated with the Salk Institute for Biological Studies, La Jolla, California. A.G. is currently affiliated with University College London, London, U.K. L.S. is currently affiliated with the Venetian Institute of Molecular Medicine, Padova, Italy.

homozygous β-*Phb2*$^{-/-}$ knockout mice throughout the study, we systematically crossed heterozygous β-*Phb2*$^{-/wt}$ (*Phb2*$^{fl/wt}$, Rip*Cre*$^{+}$) males with *Phb2*$^{fl/fl}$ (control) females. Because *Phb2*$^{fl/fl}$, Rip*Cre*$^{+}$ mice (homozygous β-*Phb2*$^{-/-}$ knockout) became diabetic at the age of 6 weeks, this strategy also avoided mating diabetic animals. As control mice, we used *Phb2*$^{fl/fl}$ littermates in order to optimize standardization of the genetic background between the groups. Cre-mediated excision of *Phb2* was assessed by PCR on genomic DNA extracted from isolated pancreatic islets using the primers 5′-ATCGTATTGGTGGCGTGCAGCA-3′ and 5′-AGGGAGGCTTGGTTTGAGGGGA-3′. Mice were maintained on a 12-h dark/light cycle and were allowed free access to standard laboratory chow (RM3-E-SQC #811181; SDS Diets, Essex, U.K.) and water. Mice were maintained in our animal facility according to procedures approved by the animal care and experimentation authorities of the Canton of Geneva.

Glucose tolerance test and hormone levels. Glucose (2 g/kg body weight) was administered intraperitoneally in 6 h–fasted mice before measurements of glucose levels on blood collected from tail vein at indicated times using a glucometer (Accu-Check; Roche Diagnostics, Rotkreuz, Switzerland). Hyperglycemia and diabetes were defined as blood glucose >11.1 mmol according to the criteria published by the American Diabetes Association (20). Plasma insulin levels from blood sampled by retro-orbital puncturing at time 0 and 15 min after glucose administration were determined using an ultrasensitive mouse insulin ELISA (Mercodia AB, Uppsala, Sweden). For plasma glucagon, blood was collected after 2-h fasting and 1-h refeeding as well as after 6-h fasting and 30 min after i.p. glucose (2 g/kg body weight) injection and glucagon levels determined by radioimmunoassay (RIA; GL-32K; Millipore, Billerica, MA).

Where indicated, mice were treated either with long-acting insulin (Levemir; Novo Nordisk, Gentofte, Denmark) injected subcutaneously twice per day (0.15 and 0.20 U in the morning and evening, respectively) or with leptin by using subcutaneous implantation of a 14-day osmotic pump (Alzet Model 1002; Alzet, Cupertino, CA) releasing 10 μg/day human leptin (Bachem, Bubendorf, Switzerland).

Islet morphology, α- and β-cell mass, and mitochondrial morphology. Pancreata were excised, weighed, fixed for 2 h in 4% paraformaldehyde, and finally embedded in paraffin. Sections of 5 μm separated by at least 250 μm were stained for insulin and glucagon using guinea pig anti-insulin (1:400) and mouse antiglucagon (1:500) primary antibodies as described (21). Fluorochrome-linked secondary antibodies were used for visualization, and images were captured by confocal microscopy (LSM 510 Meta; Carl Zeiss, Feldbach, Switzerland).

For assessment of α- and β-cell mass, sections at an interval of 250 μm throughout the pancreas were stained for glucagon and insulin, respectively, with the aforementioned primary antibodies. Horseradish peroxidase–conjugated secondary antibodies were used in order to reveal α- and β-cells by diaminobenzidine staining, and hematoxylin was used for counterstaining (21). Sections were scanned by digital microscopy (Nikon Coolscope; Nikon, Egg, Switzerland), quantification was achieved using ImageJ software (National Institutes of Health; http://rsb.info.nih.gov/nih-image/), and α- and β-cell mass was calculated as previously described (22).

For mitochondrial morphology, dispersed islet cells were allowed to adhere in culture to poly-L-lysine–coated slides before fixation and immunostaining with primary antibodies anti-TOM20 (1:100; Santa Cruz Biotechnology, Santa Cruz, CA) and anti-insulin (1:400; Sigma-Aldrich, St. Louis, MO), followed by Alexa 488– and -647–conjugated secondary antibodies, respectively. For each channel, *z*-axis stacks separated by 0.36 μm were acquired using a Zeiss LSM 510 Meta microscope with a 63 × 1.4 NA Plan Apochromat objective (Zeiss). Three-dimensional reconstruction as well as quantification of mitochondrial length was performed with the help of ImageJ software (National Institutes of Health) by manually measuring length of mitochondria in a randomly selected two-dimensional *z*-stack.

For ultrastructural analysis, isolated islets and whole pancreas of *Phb2*$^{fl/fl}$ and β-*Phb2*$^{-/-}$ mice were fixed in 2.5% glutaraldehyde in 0.1 mol/L phosphate buffer, by either immersion (islets, pancreas) or in situ perfusion (pancreas). After postfixation in 1% osmium tetroxide, all samples were processed for transmission electron microscopy as per standard procedures. Sections were analyzed in a CM10 Philips electron microscope (Philips).

Isolation of islets and measurements of their hormones. Pancreatic islets were isolated by collagenase digestion as described (23) and cultured overnight in RPMI 1640 medium supplemented with 5% heat-inactivated FCS, 10 mmol HEPES, 1 mmol sodium pyruvate, 50 μmol β-mercaptoethanol, and antibiotics in nonadherent petri dishes. For static incubation studies, overnight cultured islets were preincubated with Krebs-Ringer bicarbonate HEPES (KRBH) buffer supplemented with 2.8 mmol glucose and 0.1% BSA for 1 h (23). Then, batches of 10 islets were hand-picked and incubated with basal 2.8 mmol and stimulatory 22.8 mmol glucose at 37°C for 1 h. At the end of the incubation period, supernatants were collected, and islets were resuspended in acid/ethanol for determination of insulin concentrations. For in vitro recombination experiments, islets isolated from adult *Phb2*$^{fl/fl}$ mice were treated overnight either with control (Ad-LacZ)– or Cre-recombinase (Ad-RipCre)–expressing adenoviruses as described previously (24). The genomic deletion of *Phb2* was confirmed 24 h after transduction by PCR as described previously (18). GSIS was tested, as mentioned earlier, 72 h after transduction. Additionally, in situ pancreatic perfusions were performed in anesthetized mice following a previously published procedure (23). Insulin concentrations in supernatants, perfusates, extracted islets, and pancreata were measured using RIA (Millipore). Total pancreatic glucagon contents were determined by glucagon RIA (Millipore).

Measurements of ATP, mitochondrial membrane potential, and Ca^{2+} in isolated islets. Following overnight culture, islets were hand-picked and preincubated in KRBH at 2.8 mmol glucose for 1 h and then incubated at basal 2.8 mmol and stimulatory 22.8 mmol glucose for 15 min at 37°C before measurements of ATP levels as described previously (23).

For mitochondrial membrane potential, isolated islets were placed in 96-well plates for recording of rhodamine-123 signal (Fluostar Optima; BMG Labtech, Offenburg, Germany), maintained in KRBH with 2.8 mmol/L glucose before addition of stimulatory glucose concentration (final 22.8 mmol) according to published protocol (25).

For cellular Ca^{2+} measurements, isolated islets were allowed to adhere on poly-L-lysine–coated coverslips during overnight culture. Then, islets were incubated with 5 μmol/L Fura-2/AM in KRBH containing 2.8 mmol/L glucose and 0.02% pluronic acid for 30 min at 37°C, washed, and further incubated for 30 min in 2.8 mmol/L glucose KRBH. Coverslips were placed in a thermostatic chamber (Harvard Apparatus, Holliston, MA) maintained at 37°C, and images were acquired using an oil-immersion objective (40×) on an Axiovert microscope (Zeiss) as detailed previously (26).

Immunoblotting. Overnight cultured islets were washed once with PBS and lysed in standard RIPA buffer supplemented with protease inhibitor cocktail (Roche). Proteins were separated by SDS-PAGE and transferred onto nitrocellulose membranes. Primary antibodies used were directed against Phb1 and Phb2 (1:1,000; BioLegend, San Diego, CA), cleaved caspase-3 (1:1,000; Cell Signaling Technology, Danvers, MA), Opa1 (1:1,000; BD Biosciences, San Jose, CA), mitochondrial OXPHOS components (1:500; Mitosciences, Eugene, OR), and 4-hydroxynonenal (1:1,000; Abcam, Cambridge, U.K.). Isotype-matched HRP-conjugated secondary antibodies were used, and proteins were visualized by enhanced chemiluminescence (GE Healthcare, Glattbrugg, Switzerland). Densitometry analysis of different blots for mitochondrial complexes was performed with the help of Quantity One software (Bio-Rad, Hercules, CA).

TUNEL assay. TUNEL assay was performed on 15-min proteinase K–pretreated deparaffinized pancreas sections according to the manufacturer's protocol by using the Apoptag Fluorescein apoptosis detection kit (S7110; Chemicon, Millipore, MA). Anti-insulin primary antibody (1:400) and its appropriate fluorochrome-coupled secondary antibody (1:500) were used to label β-cells. Nuclei were counterstained with DAPI.

mtDNA copy number. Quantification of mtDNA copy number was achieved by quantitative PCR. Briefly, DNA was extracted from overnight cultured islets using the DNeasy Blood and Tissue kit (Qiagen, Düsseldorf, Germany) according to the manufacturer's protocol. Nuclear and mtDNA copy numbers were assessed by quantitative PCR using primers targeted toward the COX1 gene (for mtDNA) and nuclear RNAse P (for nuclear DNA).

RESULTS

Generation and characterization of β-*Phb2*$^{-/-}$ mice. First, we documented the expression of prohibitins in human islets by immunoblotting (Fig. 1*A*). Next, we generated mice lacking β-cell *Phb2* (β-*Phb2*$^{-/-}$) by crossing *Phb2*$^{fl/fl}$ animals carrying a floxed *Phb2* allele (18) with *Tg(Ins2-cre)*^{1Herr} mice, expressing Cre-recombinase under the control of an insulin promoter (19). PCR amplification across the *Phb2* locus generated a *Phb2*-deleted fragment in islets of β-*Phb2*$^{-/-}$ mice, but not in those of *Phb2*$^{fl/fl}$ littermate controls, showing efficient Cre-mediated recombination (Fig. 1*B*). Consistent with genomic deletion, there was a near-total ablation of Phb2 protein in β-*Phb2*$^{-/-}$ islets (Fig. 1*C*). The residual Phb2 expression observed in knockout islets is presumably accounted for by expression of the protein in non–β-cells and/or the persistence of the few β-cells that had escaped recombination. In islets isolated from β-*Phb2*$^{-/-}$ mice, loss of Phb2 was accompanied by reduced levels of its homolog Phb1 (Fig. 1*C*), as previously observed (18). This reveals the interdependence

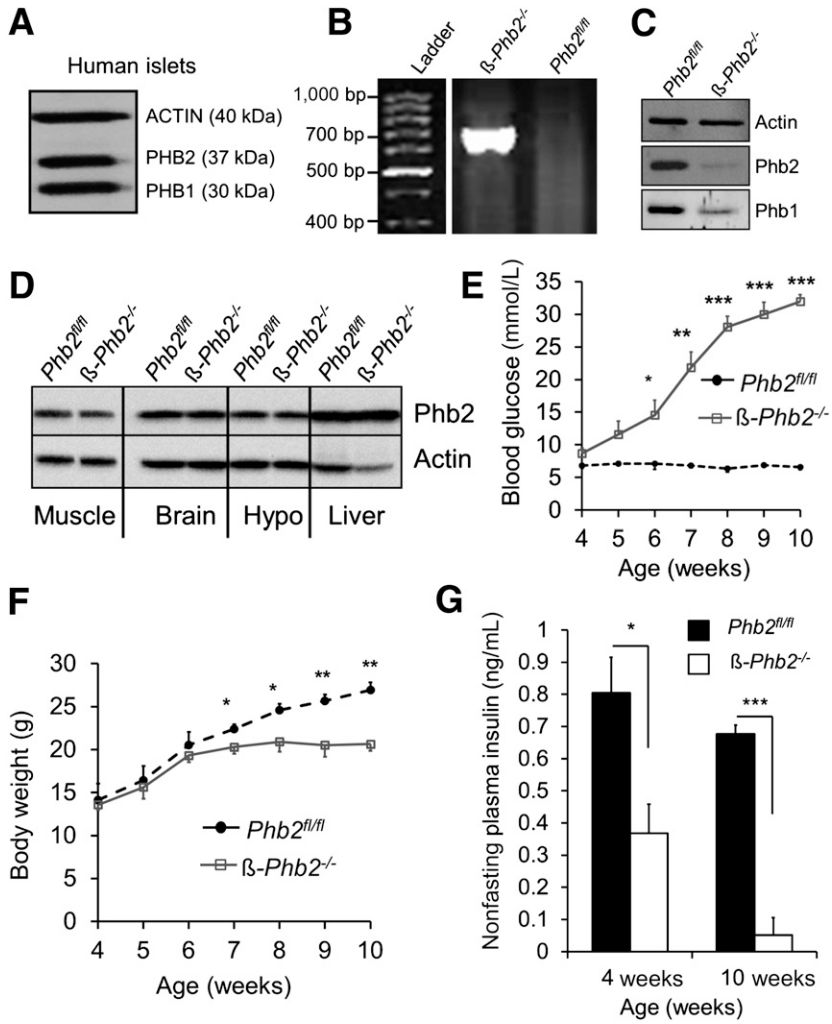

FIG. 1. β-Cell–specific deletion of *Phb2* renders mice diabetic. *A*: Abundance of Phb1 and -2 proteins in human islets revealed by immunoblotting. *B*: Recombination of *Phb2* allele was assessed by PCR on DNA extracted from isolated islets of 4-week-old β-*Phb2*$^{-/-}$ and littermate control mice. *C*: Representative immunoblotting analysis showing expression of Phb1 and Phb2 proteins in islets of control and knockout mice. β-Actin was used as loading control. *D*: Assessment of nonspecific loss of Phb2 in other tissues such as skeletal muscle, brain, hypothalamus (Hypo), and liver by immunoblotting (representative of three immunoblottings performed on tissues isolated from three mice of each genotype). *E*: Nonfasting glycemia recorded once every week between 9:00 and 10:00 A.M. from the age 4 weeks in β-*Phb2*$^{-/-}$ (□) and littermate *Phb2*$^{fl/fl}$ (●) male mice (n = 6/group). *F*: Body weights of β-*Phb2*$^{-/-}$ (□) and littermate *Phb2*$^{fl/fl}$ (●) mice measured once a week (n = 6 for each group). *G*: Nonfasting plasma insulin measured at 4 and 10 weeks of age in β-*Phb2*$^{-/-}$ (white bars) and littermate *Phb2*$^{fl/fl}$ (black bars) mice (n = 4/genotype). Data are expressed as means ± SEM. *P < 0.05, **P < 0.01, ***P < 0.001; control *Phb2*$^{fl/fl}$ versus knockout β-*Phb2*$^{-/-}$.

of these proteins and the existence of functional prohibitin complexes in β-cells. Misexpression of Rip-Cre transgene in brain and hypothalamus has been noticed in a *Tg(Ins2-cre)*^{25Mgn} transgenic line (27), although not particularly in the *Tg(Ins2-cre)*^{1Herr} (19) used in the current study (28). Consistent with these reports, Phb2 loss in β-*Phb2*$^{-/-}$ mice was restricted to pancreatic β-cells without apparent ablation in the brain, including the hypothalamus (Fig. 1*D*).

Monitoring of nonfasting glycemia in β-*Phb2*$^{-/-}$ and littermate control *Phb2*$^{fl/fl}$ mice showed normoglycemia in 4-week-old β-*Phb2*$^{-/-}$ males. However, at the age of 6 weeks, knockout mice became hyperglycemic (>11.1 mmol), thereafter progressing to strong hyperglycemia (>25 mmol) and severe diabetes (weight loss) over a 3-week period (Fig. 1*E*). Similar phenotypes were observed in female β-*Phb2*$^{-/-}$ mice (Supplementary Fig. 1). Recordings of body weight showed growth impairment starting at the age of 7 weeks, with no further weight gain compared with control littermates (Fig. 1*F*). Nonfasting hypoinsulinemia (54% less plasma insulin than control) displayed by 4-week-old β-*Phb2*$^{-/-}$ mice (Fig. 1*G*) was further lowered at 10 weeks of age (88% less than age-matched control). Heterozygous *Phb2* knockout (β-*Phb2*$^{wt/-}$) mice grew similarly to *Phb2*$^{fl/fl}$ (data not shown) and had a normal life span, whereas homozygous β-*Phb2*$^{-/-}$ mice died at the age of 12–15 weeks suffering of overt diabetes.

Phb2 loss in β-cells gradually altered glucose homeostasis in β-*Phb2*$^{-/-}$ mice. At 3 weeks of age, an intraperitoneal glucose tolerance test resulted in similar glycemic excursions in β-*Phb2*$^{-/-}$ mice and control littermates (Fig. 2*A*). One week later, mice exhibited impaired blood glucose clearance along with normal fasting glycemia (Fig. 2*B*), indicating a prediabetic state. At 6 weeks of age, β-*Phb2*$^{-/-}$ mice became severely diabetic with fasting hyperglycemia at ~15 mmol/L (Fig. 2*C*). This timing of sequential alterations (normoglycemia followed by glucose intolerance and ultimately diabetes) was consistently observed in various litters. Thus, in this mouse model, the etiology of diabetes could be followed within a short time

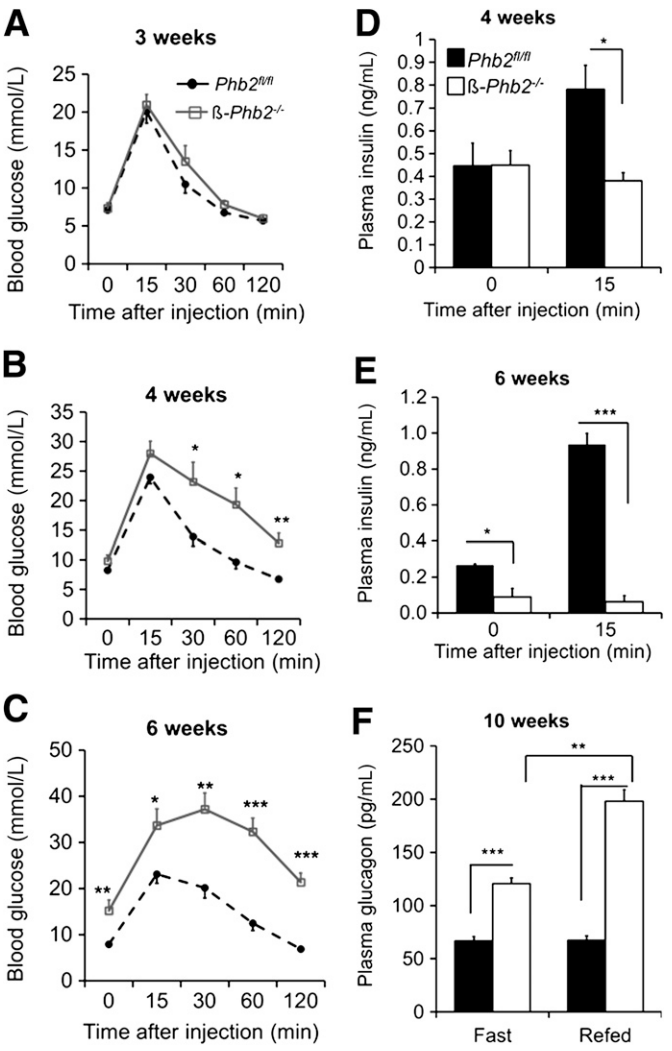

FIG. 2. Loss of Phb2 in β-cells induces development of diabetes over a 3-week period in β-*Phb2*$^{-/-}$ mice. *A–C*: Glucose tolerance test (2 g/kg) in 6 h–fasted β-*Phb2*$^{-/-}$ (□) and littermate *Phb2*$^{lox/lox}$ (●) mice. Three-week-old β-*Phb2*$^{-/-}$ (n = 6) and *Phb2*$^{fl/fl}$ (n = 4) mice (*A*), 4-week-old β-*Phb2*$^{-/-}$ (n = 7) and *Phb2*$^{fl/fl}$ (n = 6) (*B*), and 6-week-old β-*Phb2*$^{-/-}$ (n = 7) and *Phb2*$^{fl/fl}$ (n = 7) (*C*) mice. *D* and *E*: In addition to blood glucose, plasma insulin levels were determined before and 15 min after glucose injection. β-*Phb2*$^{-/-}$ (white bars) and littermate *Phb2*$^{fl/fl}$ (black bars) mice. At 4 weeks of age, β-*Phb2*$^{-/-}$ (n = 6) and *Phb2*$^{fl/fl}$ (n = 5) (*D*) and 6-week-old β-*Phb2*$^{-/-}$ (n = 3) and *Phb2*$^{fl/fl}$ (n = 4) animals (*E*). *F*: At 10 weeks of age, plasma glucagon levels were determined after 2-h fasting and subsequent 1-h refeeding. β-*Phb2*$^{-/-}$ (white bars) and littermate *Phb2*$^{fl/fl}$ (black bars) mice (n = 4/group). Data presented are means ± SEM. *P < 0.05, **P < 0.01, ***P < 0.001 between the two groups.

span of ~3 weeks. Heterozygous β-*Phb2*$^{wt/-}$ mice had normal glucose excursions even at the age of 10 weeks (Supplementary Fig. 2), indicating that the observed phenotype in β-*Phb2*$^{-/-}$ mice was not mediated by the Rip-*Cre* allele present as a single allele in both heterozygous β-*Phb2*$^{wt/-}$ and homozygous β-*Phb2*$^{-/-}$ mice.

We further ascertained the possible impairment of insulin delivery suggested by low nonfasting plasma insulin levels (Fig. 1*G*). In 4-week-old β-*Phb2*$^{-/-}$ mice, the plasma insulin levels observed 15 min after a glucose challenge were markedly lower (−50%) than in control mice (Fig. 2*D*). At the age of 6 weeks, β-*Phb2*$^{-/-}$ mice exhibited very low fasting as well as glucose-induced plasma insulin levels (Fig. 2*E*). Therefore, diabetes development is first revealed in 4-week-old β-*Phb2*$^{-/-}$ by glucose intolerance and lack of glucose-induced elevation of plasma insulin. Interestingly, 10-week-old β-*Phb2*$^{-/-}$ mice exhibited hyperglucagonemia following a moderate 2-h fasting. Glucagon levels were further elevated in knockout animals upon refeeding (Fig. 2*F*), although not upon a glucose i.p. challenge (Supplementary Fig. 3).

Reduced GSIS in β-*Phb2*$^{-/-}$ pancreas at 6 weeks. At the age of 6 weeks, when Phb2 knockout animals became diabetic, we performed in situ pancreatic perfusions to test the β-cell response in islets maintained in their native pancreatic environment. This revealed a dramatic reduction of GSIS when pancreas of β-*Phb2*$^{-/-}$ were compared with those of *Phb2*$^{fl/fl}$ controls (Fig. 3*A*). In the former mice, first and second phases of insulin secretion were reduced by 76 and 78%, respectively, when compared with the corresponding phases of *Phb2*$^{fl/fl}$ controls (Fig. 3*B*).

Impaired metabolism-secretion coupling in *Phb2*$^{-/-}$ β-cells. Because the chronic hyperglycemia observed by the age of 5 to 6 weeks might induce secondary changes perturbing islet function, we studied islets isolated from normoglycemic mice at the age of 3 to 4 weeks (Figs. 1*E*, 2*A* and *B*). Despite normoglycemia, insulin content in β-*Phb2*$^{-/-}$ islets was decreased by 46% when compared with that of control islets (Fig. 4*A*). Islet function tested in static incubation revealed a markedly reduced GSIS in islets

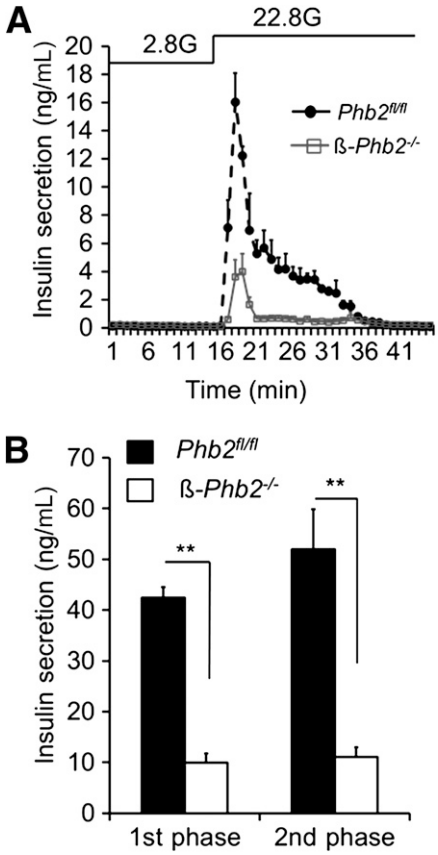

FIG. 3. Kinetics of GSIS is altered in 6-week-old β-*Phb2*$^{-/-}$ mice as revealed by in situ pancreatic perfusion. *A*: Glucose-induced insulin release determined by in situ pancreatic perfusions on 6-week-old β-*Phb2*$^{-/-}$ (□) and littermate *Phb2*$^{fl/fl}$ (●) mice. Glucose was raised from basal 2.8 mmol/L (2.8G) to stimulatory 22.8 mmol/L (22.8G). *B*: Insulin released during first phase of the glucose response (i.e., 5 min after 22.8G stimulation) and second phase (i.e., 40 min after completion of first phase of secretion). Traces show β-*Phb2*$^{-/-}$ (white bars; n = 4) and littermate *Phb2*$^{fl/fl}$ (black bars; n = 3) mice. All data are expressed as means ± SEM. **P < 0.01 between the two groups.

lacking Phb2 (Fig. 4*B* and *C*). When normalized per islet, the secretory response was 63% lower in β-*Phb2*$^{-/-}$ islets compared with controls. Normalized per insulin content, the difference was −50%, indicating that, at this stage, the lower insulin content of β-*Phb2*$^{-/-}$ islets did not account for their blunted glucose response. Accordingly, there was no significant difference between control and knockout islets when insulin secretion was stimulated by nonmetabolic KCl-induced cell depolarization (data not shown). This indicates that the exocytotic machinery downstream of Ca^{2+} signaling was preserved in β-*Phb2*$^{-/-}$ islets. However, the Ca^{2+} rise secondary to glucose stimulation requires mitochondrial activation in terms of ATP generation. Hence, we measured intracellular Ca^{2+} concentration ($[Ca^{2+}]_i$) in response to glucose stimulation in isolated islets. In comparison with littermate controls, β-*Phb2*$^{-/-}$ islets exhibited a lower $[Ca^{2+}]_i$ rise upon glucose stimulation (Fig. 4*D*), while the response to KCl, used as a Ca^{2+}-raising agent, was similar in the two groups (Supplementary Fig. 4).

Additionally, we acutely depleted Phb2 in vitro in β-cells by treating nonrecombined *Phb2*$^{fl/fl}$ islets isolated from adult mice (age 10–14 weeks) with adenovirus expressing Cre recombinase (Fig. 5*A* and *B*). Compared with control islets transduced with Ad-LacZ virus, we observed impaired GSIS in recombined Ad-RipCre treated islets 72 h after viral transduction (Fig. 5*C*). These data demonstrate that Phb2 is required for proper metabolism-secretion coupling in β-cells.

Perturbed mitochondrial morphology and function in *Phb2*-null β-cells. We next studied mitochondrial morphology in animals aged 3 to 4 weeks. Three-dimensional reconstructions of confocal microscopy *z*-stacks images of mitochondrial reticulum through entire β-cells are shown in Fig. 6*A* and Supplementary Fig. 5*A* and *B*. Normal mouse β-cell displayed tubular interconnected mitochondria. On the contrary, absence of Phb2 in β-cells resulted in fragmented mitochondrial network, revealing an average mitochondrial length ~50% shorter compared with

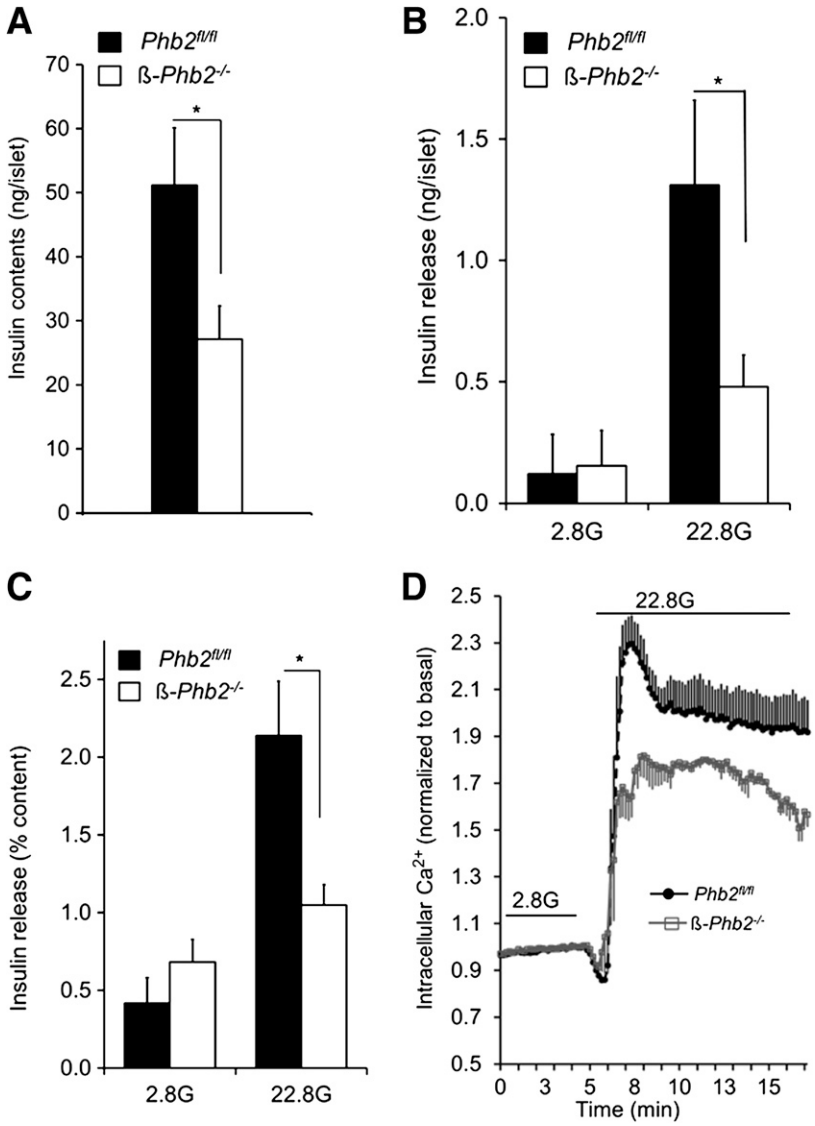

FIG. 4. Stimulus-secretion coupling is already deficient in β-cells from 4-week-old β-*Phb2*$^{-/-}$ mice. *A*: Insulin contents of islets isolated from 4-week-old β-*Phb2*$^{-/-}$ (white bars) and littermate *Phb2*$^{fl/fl}$ (black bars) mice (n = 5). *B* and *C*: GSIS tested as static incubation at basal 2.8 mmol/L (2.8G) and stimulatory 22.8 mmol/L (22.8G) glucose on islets isolated from 4-week-old mice. Insulin secretion rate is expressed as insulin release normalized per islet (*B*) and to total islet insulin content (*C*). β-*Phb2*$^{-/-}$ (white bars) and littermate *Phb2*$^{fl/fl}$ (black bars) mice (n = 5). *D*: $[Ca^{2+}]_i$ at basal 2.8G and in response to 22.8G in isolated islets from *Phb2*$^{fl/fl}$ (●) and β-*Phb2*$^{-/-}$ (□) mice. Traces show averages of recordings from three animals per genotype. Data are expressed as means ± SEM. *$P < 0.05$ between the two groups.

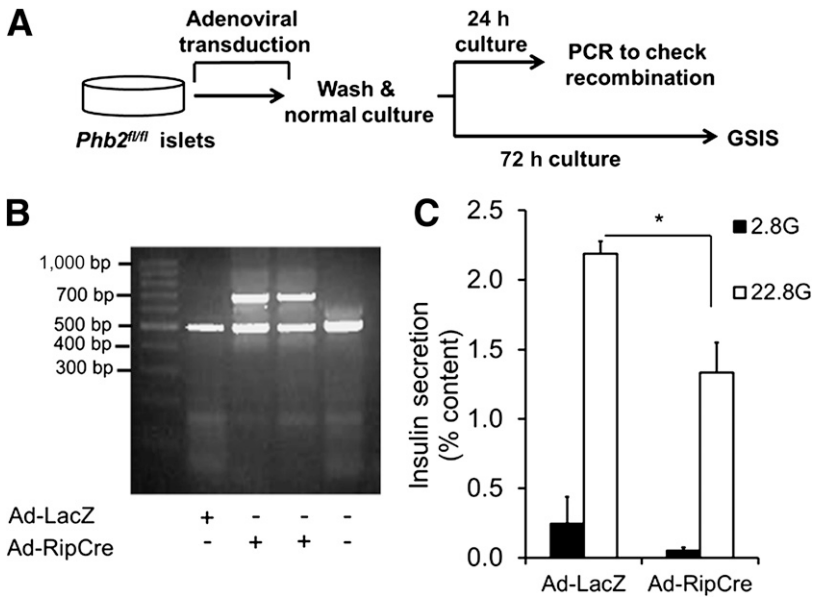

FIG. 5. Acute in vitro knockout of *Phb2* in β-cells. Islets isolated from *Phb2*$^{fl/fl}$ mice (10–14 weeks of age) were transduced with control (Ad-LacZ) or Cre-recombinase (Ad-RipCre) adenoviruses. *A*: Flow chart for in vitro recombination experiments. *B*: PCR on DNA extracted from islets treated with respective viruses showing efficient recombination (699-bp band) 24 h after overnight incubation with Ad-RipCre. *C*: Insulin release during static incubation at basal 2.8 mmol/L (2.8G) and stimulatory 22.8 mmol/L (22.8G) glucose from islets after treatment with indicated viruses ($n = 4$). Data are expressed as means ± SEM. *$P < 0.05$.

control β-cells (Fig. 6*B*). In accordance with this fragmented mitochondrial network, we observed excessive proteolytic cleavage of the long isoforms (L1 and L2) of the mitochondrial inner membrane fusion protein Opa1, resulting in the accumulation of the short isoform S5 (Fig. 6*C*). In spite of these changes, electron microscopy revealed a comparable ultrastructural appearance of mitochondria in the β-cells of 4-week-old control *Phb2*$^{fl/fl}$ and knockout β-*Phb2*$^{-/-}$ mice, whether these cells were studied in isolated islets (Fig. 6*D* and *E*) or intact pancreas (not shown). Similar observations were made in β-cells of newborn, 2-week-, and 6-week-old mice (not shown). These pictures (Fig. 6*A*, *D*, and *E*) show that mitochondrial fragmentation is not necessarily associated with alteration of mitochondrial ultrastructure.

In neuronal mitochondria, Phb2 is necessary for the maintenance of mtDNA, probably requiring Opa1-dependent mitochondrial fusion (29). In this context, we quantified mtDNA copy number normalized to nuclear DNA. This revealed a 47% reduction of the mitochondrial genome in *Phb2* null islets versus controls (Fig. 6*F*), which was accompanied by lower levels of mtDNA-encoded subunit of complex IV of the respiratory chain at the protein level (Fig. 6*G* and *H*). Alterations in the electron transport chain might favor production of reactive oxygen species (30,31). However, we recorded similar levels of 4-hydroxynonenal, an aldehydic product of lipid peroxidation commonly enhanced during oxidative stress (Supplementary Fig. 6*A* and *B*).

The mitochondrial function was assessed by measuring mitochondrial membrane potential and ATP. Upon glucose stimulation, mitochondria of Phb2 null β-cells exhibited weak hyperpolarization compared with their control counterparts (Fig. 6*I*). This was translated into impaired ATP generation after glucose stimulation. At basal 2.8 mmol/L glucose, *Phb2*$^{fl/fl}$ and β-*Phb2*$^{-/-}$ islets had similar concentrations of ATP (29.4 ± 9.2 and 28.2 ± 12.2 pmol/μg islet proteins, respectively). Upon 22.8 mmol glucose stimulation, we measured a 30% rise in ATP for control islets versus only 7% for β-*Phb2*$^{-/-}$ islets (Fig. 6*J*), which might be sufficient for the blunted elevation of $[Ca^{2+}]_i$ (Fig. 4*D*). These data show that loss of Phb2 induced alterations in mitochondrial morphology and function, resulting in an impaired metabolic response.

Progressive decline in β-cell mass and islet architecture in β-*Phb2*$^{-/-}$ mice. The defective GSIS observed in β-*Phb2*$^{-/-}$ mice might be caused by physical or functional loss of β-cells or both. Hematoxylin and eosin staining of pancreas of 4-week-old knockout mice revealed absence of infiltration of immune cells within and around islets (Supplementary Fig. 7). At the same age, immunohistochemistry showed that most islets of β-*Phb2*$^{-/-}$ mice exhibited reduced size with preserved architecture (i.e., glucagon-positive α-cells at the periphery and insulin-producing β-cells forming the core of the islet) (Fig. 7*A*). At the age of 10 weeks, however, islets were completely disorganized in β-*Phb2*$^{-/-}$ mice, with only few β-cells intermingled with α-cells (Fig. 7*B*). Quantification of islet β-cell mass in β-*Phb2*$^{-/-}$ mice revealed that β-cell loss amounted to 35% at the age of 4 weeks and >90% at the age of 10 weeks compared with age-matched controls, consistent with the corresponding alterations in pancreatic insulin content (Fig. 7*C* and *D*). In 10-week-old β-*Phb2*$^{-/-}$ mice, we observed an expanded α-cell mass compared with that seen in controls (Fig. 7*E*). This was substantiated by higher pancreatic glucagon content in β-*Phb2*$^{-/-}$ mice at 10 weeks of age compared with control animals (Fig. 7*F*).

Deficient β-cell function at 4 weeks of age, followed by loss of β-cell mass at 10 weeks in β-*Phb2*$^{-/-}$ mice, might explain the development of diabetes. In order to test if the lack of insulin delivery was a key contributor to the disease, β-*Phb2*$^{-/-}$ animals were treated with insulin. The daily administration of insulin to β-*Phb2*$^{-/-}$ diabetic mice, which was initiated at 8 weeks of age, fully corrected glycemia (Fig. 7*G*) and provided for maintenance of

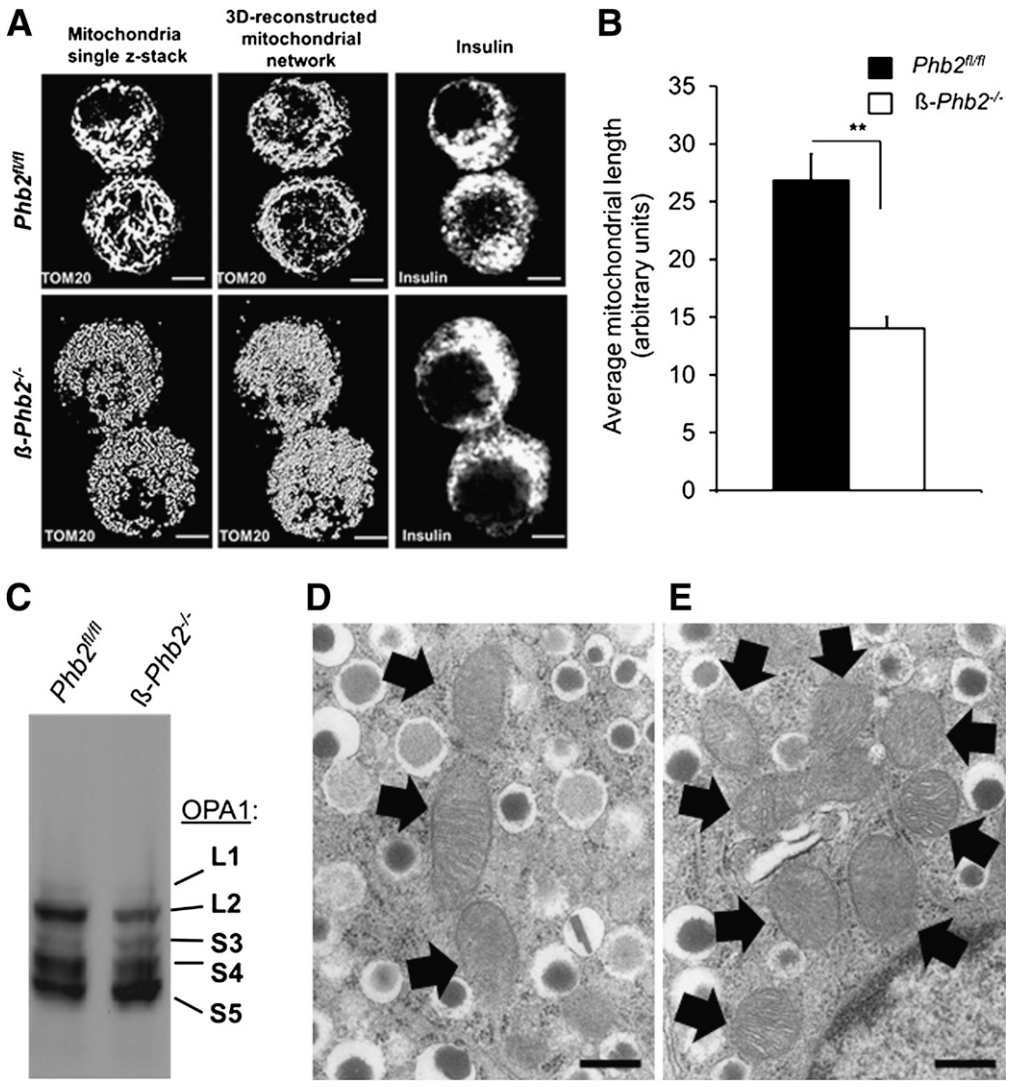

FIG. 6. Mitochondrial morphology and function in β-cells from 3- to 4-week-old β-*Phb2*$^{-/-}$ mice. *A*: Mitochondrial morphology was analyzed on dispersed pancreatic islet cells by immunofluorescence. Representative β-cells from control *Phb2*$^{fl/fl}$ and knockout β-*Phb2*$^{-/-}$ mice as indicated. Single plane showing mitochondrial network, three-dimensional (3D) reconstruction of *z*-stacks through entire β-cell, and staining of insulin. Scale bars, 2 μm. *B*: Average mitochondrial length measured on 25–40 distinct mitochondria per cell in a randomly selected two-dimensional *z*-stack. *Phb2*$^{fl/fl}$ (n = 27) and *Phb2*$^{-/-}$ (n = 21) β-cells from different mice (n = 3) of each genotype were analyzed. *C*: Representative immunoblotting showing increased proteolysis of long isoforms of mitochondrial fusion protein Opa1 in *Phb2*$^{-/-}$ islets compared with controls. Electron microscopy of β-cells in islets isolated from 4-week-old control *Phb2*$^{fl/fl}$ (*D*) and knockout β-*Phb2*$^{-/-}$ mice (*E*). The structure of mitochondria (arrows) appeared normal in the two mouse genotypes. Scale bars, 200 nm. *F*: mtDNA copy number in islets isolated from respective genotypes. DNA copies of mitochondrial complex I was normalized to the DNA levels of nuclear *RNAseP* (nDNA). n = 3 and n = 5 for *Phb2*$^{fl/fl}$ and β-*Phb2*$^{-/-}$, respectively. *G*: Two independent representative immunoblots showing mitochondrial respiratory chain complexes (C) of isolated islets using antibody cocktail targeted toward different subunits (C-I, NDUFB8; C-II, iron-sulfur protein; C-III, core protein 2; C-IV, subunit-I; and C-V, ATP synthase subunit-α). *H*: Densitometry analysis of three independent blots. β-*Phb2*$^{-/-}$ (white bar; n = 4) and *Phb2*$^{fl/fl}$ (black bar; n = 3). *I*: Mitochondrial membrane potential (Δψm) in islets isolated from respective genotype was measured with rhodamine123. Fluorescence intensity was recorded during incubations at 2.8 mmol (basal) glucose and subsequently at 22.8 mmol (stimulated) glucose. Triplicates of 10 islets from each animal were used in independent experiments. β-*Phb2*$^{-/-}$ (□) and littermate *Phb2*$^{fl/fl}$ mice (●); n = 3. *J*: Cellular ATP levels were measured after incubating 50 islets each at 2.8 mmol glucose and stimulatory 22.8 mmol glucose for 15 min. Percentage of rise in ATP production in response to stimulatory glucose concentration against basal glucose concentrations was calculated. *Phb2*$^{fl/fl}$ (black bar) n = 5 and β-*Phb2*$^{-/-}$ (white bar) n = 4. Data on panels *B*, *F*, *H*, *I*, and *J* are means ± SEM. Immunofluorescence and immunoblotting images are representative of at least three independent analyses performed on different mice. *P < 0.05, **P < 0.01 between the two groups. a.u., arbitrary units.

control body weights (Fig. 7*H*) for the 10-week period of the treatment. Untreated β-*Phb2*$^{-/-}$ mice were killed at 11 weeks of age because of a severe diabetic state with dramatic loss of body weight. Incidentally, the rescue by insulin treatment of multiple alterations of the β-*Phb2*$^{-/-}$ mice shows the absence of a hypothalamic contribution to the observed phenotype. Leptin therapy in diabetic mice has been shown to normalize glycemia through suppression of hyperglucagonemia (32). In view of the higher α-cell mass and pancreatic glucagon of β-*Phb2*$^{-/-}$ mice (Fig. 7*E* and *F*), we tested leptin treatment in these animals. Fig. 7*I* shows that subcutaneous delivery of leptin over a 10-day period partially corrected glycemia in 8-week-old diabetic β-*Phb2*$^{-/-}$ mice.

β-Cell apoptosis and proliferation in β-*Phb2*$^{-/-}$ mice. Islets isolated from 4-week-old β-*Phb2*$^{-/-}$ mice exhibited a marked upregulation of caspase-3 cleavage compared with age-matched controls (Fig. 8*A*). Additionally, these cells were more susceptible to apoptotic stimuli, such as staurosporine (Fig. 8*A*). On pancreas sections, we typically

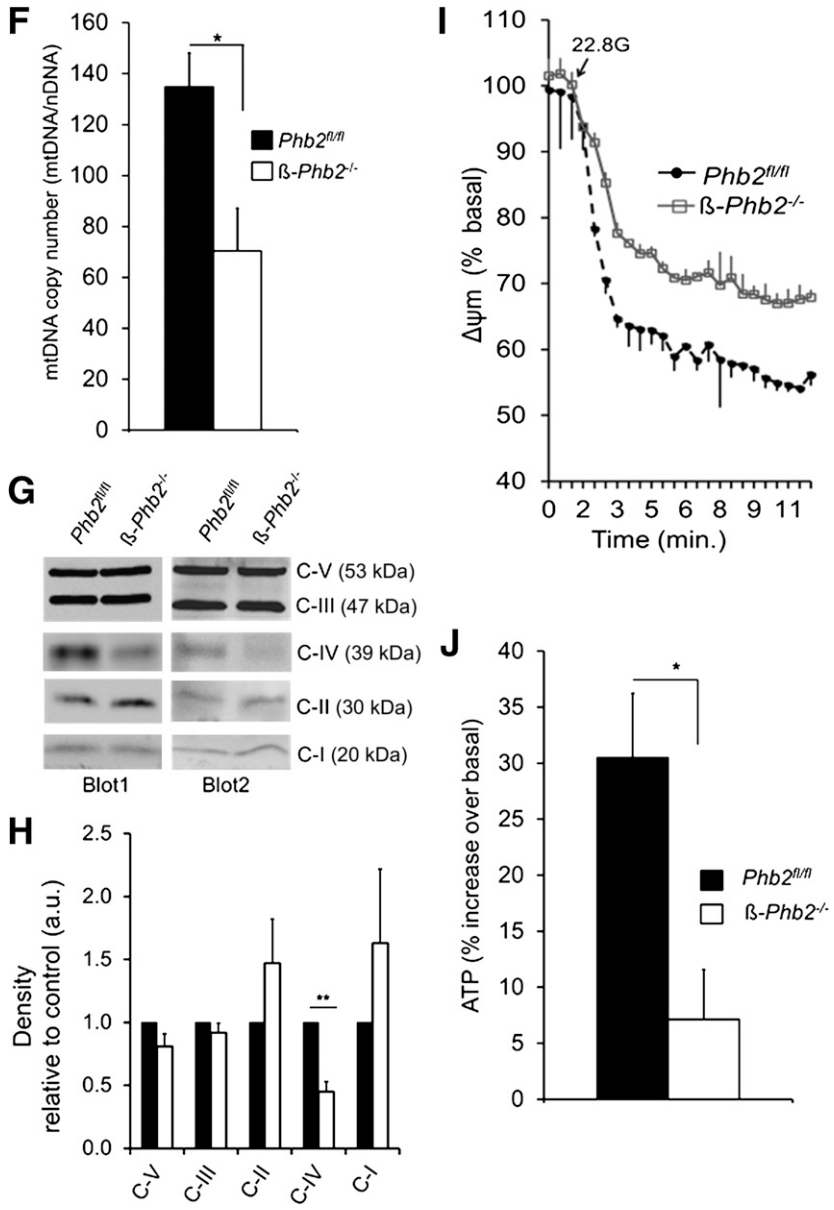

FIG. 6. Continued.

observed one to three apoptotic β-cells by TUNEL assay in β-*Phb2*$^{-/-}$ islets, while we detected none in control islets (Fig. 8*B*). Given that β-*Phb2*$^{-/-}$ mice maintained a sufficient β-cell mass up to the age of 4 weeks, before the rapid development of diabetes, data suggest the involvement of some compensatory mechanism.

Preservation of ~65% of the β-cell mass in 4-week-old β-*Phb2*$^{-/-}$ mice (Fig. 7*C*) despite active apoptosis (Fig. 8*A* and *B*), prompted us to investigate β-cell proliferation. Quantification of Ki-67–positive β-cells in control mice showed the expected 1% proliferating β-cells at the age of 4 weeks (Fig. 8*C*). Surprisingly, we observed an increased number of Ki-67–positive nuclei within insulin-positive cells of β-*Phb2*$^{-/-}$ mice (Fig. 8*C*). This resulted in a 2.5-fold β-cell proliferation increment in β-*Phb2*$^{-/-}$ mice versus control (Fig. 8*D*). However, at the age of 10 weeks, the 90% reduction in β-cell mass of β-*Phb2*$^{-/-}$ mice (Fig. 7*C*) suggested loss of such a compensatory proliferation.

DISCUSSION

The current study documents the expression of prohibitins and their importance for β-cell function and survival. Ablation of *Phb2* in mouse β-cells sequentially resulted in impaired mitochondrial function and insulin secretion, loss of β-cells, progressive alteration of glucose homeostasis, and ultimately severe diabetes. Defective insulin supply was contributed by both β-cell dysfunction and apoptosis, suggesting a pivotal role for Phb2 in maintenance of the β-cell integrity. At the molecular level, we observed that deletion of Phb2 caused mitochondrial abnormalities such as reduction of mtDNA copy number and complex IV levels. Our β-*Phb2*$^{-/-}$ mice share some phenotypic similarities with β-cell–specific *frataxin* knockout. Frataxin is located in the mitochondrial matrix, controlling iron-sulfur cluster assembly (33). Mice lacking frataxin in β-cells are born healthy but subsequently develop glucose intolerance and then diabetes by the age of 9 months, explained by

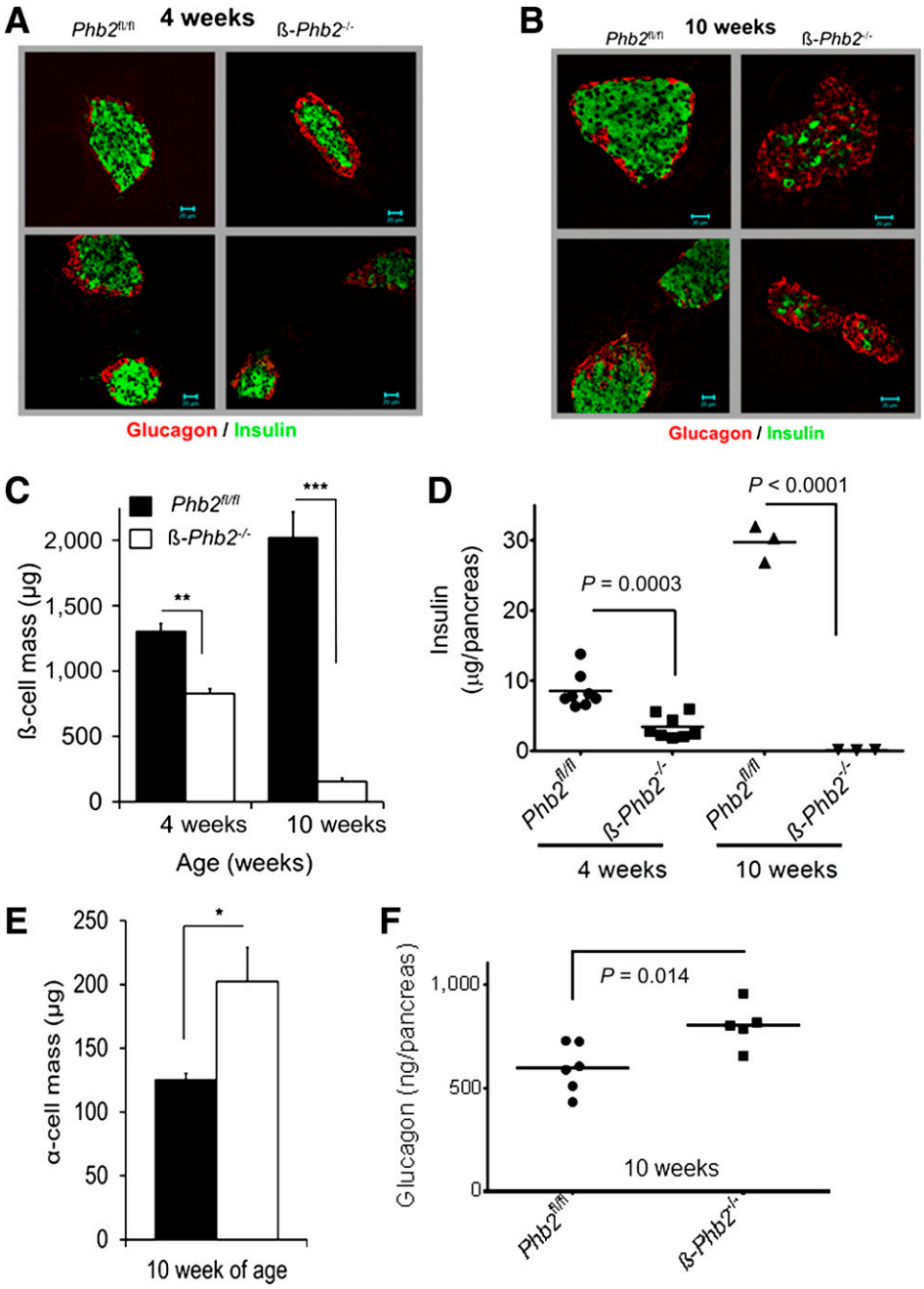

FIG. 7. Lack of Phb2 in β-cells alters islet cell composition and architecture. *A* and *B*: Representative immunohistochemistry images of pancreatic sections from β-*Phb2*$^{-/-}$ and littermate *Phb2*$^{fl/fl}$ mice with insulin stained in green and glucagon in red. *Top panels* show individual islets while *bottom panels* show two islets in close proximity. Scale bars, 20 µm. Four-week-old (*A*) and 10-week-old mice (*B*), representative of three independent analyses performed on three different mice of each genotype per time point. *C*: Total pancreatic β-cell mass calculated at the age of 4 and 10 weeks from β-*Phb2*$^{-/-}$ (white bar) and littermate *Phb2*$^{fl/fl}$ (black bar) mice. $n = 3$ for each genotype. *D*: Total pancreatic insulin contents from β-*Phb2*$^{-/-}$ and littermate *Phb2*$^{fl/fl}$ mice at the age of 4 and 10 weeks; $n = 8$ and 3 per genotype for animals at the age of 4 weeks (●, *Phb2*$^{fl/fl}$; ■, β-*Phb2*$^{-/-}$) and 10 weeks (▲, *Phb2*$^{fl/fl}$; ▼, β-*Phb2*$^{-/-}$), respectively. *E*: Total pancreatic α-cell mass at the age of 10 weeks from β-*Phb2*$^{-/-}$ (white bar) and littermate *Phb2*$^{fl/fl}$ (black bar) mice; $n = 3$/genotype. *F*: Total pancreatic glucagon contents from β-*Phb2*$^{-/-}$ (■) and littermate *Phb2*$^{fl/fl}$ (●) mice at the age of 10 weeks; *Phb2*$^{fl/fl}$ ($n = 6$) and β-*Phb2*$^{-/-}$ ($n = 5$). Nonfasting glycemia (*G*) and body weights (*H*) of β-*Phb2*$^{-/-}$ mice measured once a week at 5:00 P.M. from age of 7 weeks onward. Long-acting insulin was injected subcutaneously twice a day (◇, gray zone, $n = 3$). Nontreated β-*Phb2*$^{-/-}$ mice (●, $n = 2$) were killed at the age of 11 weeks due to end-stage diabetic state. *I*: Glycemia of 4 h–fasted β-*Phb2*$^{-/-}$ mice at indicated time points after subcutaneous implantation at the age of 8 weeks of 14-day osmotic pump releasing either 10 µg/day of leptin (◇, $n = 3$) or saline (●, $n = 2$). All data are expressed as means ± SEM. *$P < 0.05$, **$P < 0.01$, ***$P < 0.001$; control (*Phb2*$^{fl/fl}$) versus β-*Phb2*$^{-/-}$.

oxidative stress, apoptosis, and then reduced islet mass (31). Phb2 deficiency caused more rapid development of diabetes across the age of 3 to 6 weeks, also accompanied by β-cell loss but without apparent oxidative stress.

Phb2-null β-cells exhibited short, fragmented, and globular mitochondria, which, however, retained a normal ultrastructural appearance, as judged by the persistence of a double membrane boundary and numerous thin elongated cristae. This was nevertheless associated with mitochondrial dysfunction, as shown by reduced glucose-induced ATP production. *Phb2* knockout β-cells had accelerated proteolytic degradation of L-Opa1 isoforms.

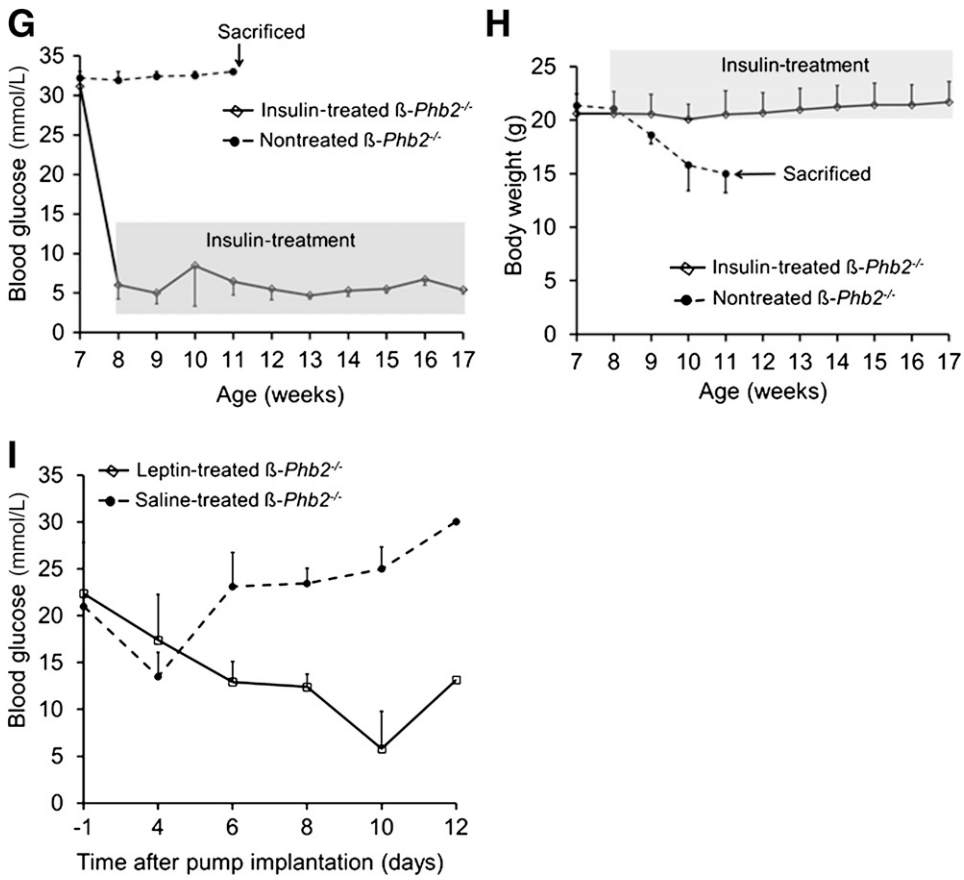

FIG. 7. Continued.

Indeed, we observed the accumulation of the short Opa1 isoform S5, when a balanced proportion of short and long forms is necessary for the proper function of this protein (16). Deletion of Opa1 in mouse β-cells decreases the activity of electron transport chain complex IV and alters ATP generation (9). The present data indicate that a selective loss of L-Opa1, and/or the accumulation of its short isoform, results in mitochondrial pattern distinct from complete ablation of Opa1 (9). Fragmented mitochondrial pattern has been documented in β-cells of human type 2 diabetic subjects and animal models for diabetes (8,34,35). However, it was unclear from these studies whether the alterations in mitochondrial morphology were the cause or consequence of diabetes. Strikingly, alterations of mitochondria appeared well before the onset of diabetes in β-*Phb2*$^{-/-}$ mice. Therefore, our data favor a role for Phb2 in Opa1-dependent mitochondrial fusion for β-cell function and morphology.

We measured lower mtDNA copy number and complex IV levels in β-*Phb2*$^{-/-}$ islets. In *Opa1*-null islets, mtDNA copies are unchanged (9). However, in neurons lacking Phb2, destabilization of L-Opa1 is associated with progressive loss of the mitochondrial genome (29), pointing to a complex equilibrium between the Opa1 isoforms for the maintenance of mtDNA integrity. In β-*Phb2*$^{-/-}$ islets, degradation of L-Opa1 accompanied by a decline in mtDNA might explain the marked reduction in the glucose response, which was more severe than in the complete absence of Opa1 (9).

Mitochondrial abnormalities were present in the β-cells of β-*Phb2*$^{-/-}$ mice, rendering these animals severely diabetic by the age of 6 weeks. The lower insulin release of β-*Phb2*$^{-/-}$ mice was also contributed by reduced β-cell mass, although at the age of 4 weeks, the secretory response was decreased independently of insulin content and specifically for mitochondrion-dependent secretagogue. Glucose intolerance appeared at this age of 4 weeks when β-cell mass in β-*Phb2*$^{-/-}$ mice was still ~65% of control animals, whereas hyperglycemia developed 2 weeks later. Clinical data have documented the maintenance of glucose tolerance in healthy donors of functional islets who underwent partial pancreatectomy (36). Interestingly, a recent study in humans reported that diabetes appears after a reduction in β-cell mass of ~65%, while postchallenge glucose excursions in prediabetic subjects exhibit glucose intolerance before this critical threshold is reached (37). Therefore, within a 2- to 3-week period, the β-*Phb2*$^{-/-}$ mouse model recapitulates the progressive stages of human diabetes, with progression from β-cell impairment associated with glucose intolerance to diabetes with fasting hyperglycemia.

In mouse embryonic fibroblasts lacking Phb2 (18), as well as in *Opa1*-null β-cells (9), apoptosis is not increased (unless stimulated by extrinsic stimuli), although the proliferative capacity of β-cells is lost. In marked contrast, the 4-week-old β-*Phb2*$^{-/-}$ mice exhibited a higher β-cell proliferation, which partially compensated the enhanced apoptosis during the first weeks of life. Apoptotic TUNEL-positive β-cells were regularly observed in islets of β-*Phb2*$^{-/-}$ mice, while such events were extremely rare in control mice. This suggests that β-*Phb2*$^{-/-}$ mice gradually lost β-cells by apoptosis over a period of

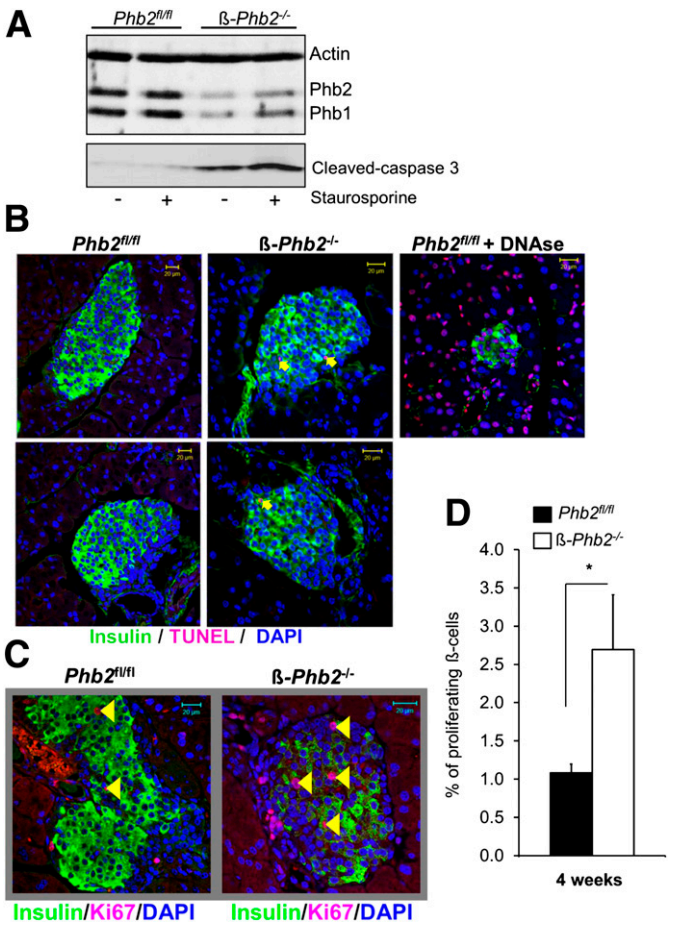

FIG. 8. Both apoptosis and proliferation of β-cells induced in β-*Phb2*$^{-/-}$ mice at 4 weeks of age. *A*: Representative immunoblotting for apoptosis analysis showing increased levels of cleaved caspase-3 in islets of β-*Phb2*$^{-/-}$ versus control *Phb2*$^{fl/fl}$ mice. Islets were treated (+) or not (−) with 1 μmol/L staurosporine for 4 h before analysis. Representative of three independent analyses performed on different mice. *B*: Representative images of three independent experiments of immunofluorescence on pancreatic sections showing labeling of TUNEL-positive β-cells in islets of β-*Phb2*$^{-/-}$ and littermate *Phb2*$^{fl/fl}$ mice at the age of 4 weeks. The TUNEL marker antidigoxin was stained in pseudo-color red, appearing in pink due to overlapping with blue-colored DAPI staining showing nucleus. Insulin was stained in green. TUNEL-positive nuclei are highlighted by yellow arrows. Pancreatic sections from control mice that were treated with DNAse show extensive TUNEL labeling in endocrine and exocrine region. *C*: Representative images of immunofluorescence on pancreatic sections showing β-cell proliferation in islets of β-*Phb2*$^{-/-}$ and littermate *Phb2*$^{fl/fl}$ mice at the age of 4 weeks. The proliferation marker Ki-67 was stained in red, appearing in pink due to DAPI staining overlap and revealing nuclear localization. Insulin was stained in green and DAPI in blue. Ki-67–positive nuclei are highlighted by yellow arrowheads. *D*: β-Cell proliferating index is expressed as percent of proliferating β-cells after computing Ki-67–positive nuclei for 1,000 β-cells analyzed per mouse at the age of 4 weeks in both β-*Phb2*$^{-/-}$ (white bar) and control *Phb2*$^{fl/fl}$ (black bar). Data expressed as means ± SEM. **P* < 0.05; *n* = 3/genotype.

~10 weeks. Enhanced apoptosis mediated by cleavage of caspase-3 was a likely consequence of Phb2 deletion rather than Opa1 degradation, since caspase-3 is not activated in *Opa1*-null β-cells (9).

In this study, we also observed the expansion of the α-cell mass and pancreatic glucagon content in 10-week-old β-*Phb2*$^{-/-}$ mice. In diabetic patients, loss of β-cells accompanied by an increase in α-cell mass has been documented and might contribute to hyperglucagonemia, precipitating hyperglycemia because of increased hepatic glucose production (38). Interestingly, after 2 h of fasting, β-*Phb2*$^{-/-}$ mice exhibited hyperglucagonemia, which was further enhanced following food ingestion. Moreover, leptin treatment partially corrected glycemia in diabetic β-*Phb2*$^{-/-}$ mice, in accordance with a glucagon-suppressor effect of leptin (38). These findings support the growing interest in α-cell as a critical therapeutic target for the treatment of diabetes.

β-*Phb2*$^{-/-}$ mice represent a unique model of spontaneous diabetes development, through a series of molecular events appearing over a 3-week period, not requiring the administration of toxic diets or chemicals. Overall, our data demonstrate that Phb2 is essential for the function and survival of β-cells. Phb2 regulates mitochondria by preserving some of their key components such as mtDNA, respiratory chain subunits, and the morphology regulator L-Opa1. Phb2 ablation impairs mitochondrial activation, rendering β-cells unresponsive to glucose and ultimately leading to apoptosis, which promotes β-cell loss and diabetes.

ACKNOWLEDGMENTS

This work was supported by the Swiss National Science Foundation (grants 310030B_135704 to P.Ma. and 310030_141162 to P.Me.) and the State of Geneva.

No potential conflicts of interest relevant to this article were reported.

S.S. conducted experiments, analyzed data, and wrote the manuscript. F.T., L.S., and P.Me. developed specific techniques and analyzed corresponding data. C.M., P.L.H., and T.L. generated transgenic animals essential for this study. A.G. generated data. P.Ma. supervised the project, analyzed data, and wrote the manuscript. P.Ma. is the guarantor of this work and, as such, had full access to all the data in the study and takes responsibility for the integrity of the data and the accuracy of the data analysis.

The authors thank Thierry Brun (University of Geneva) and Mauro Corrado (University of Geneva) for advice and helpful discussions, and Mrs. Dorothée Caille (University of Geneva) for processing the EM samples.

REFERENCES

1. Maechler P, Li N, Casimir M, Vetterli L, Frigerio F, Brun T. Role of mitochondria in beta-cell function and dysfunction. Adv Exp Med Biol 2010; 654:193–216
2. Kennedy ED, Maechler P, Wollheim CB. Effects of depletion of mitochondrial DNA in metabolism secretion coupling in INS-1 cells. Diabetes 1998;47:374–380
3. Silva JP, Köhler M, Graff C, et al. Impaired insulin secretion and beta-cell loss in tissue-specific knockout mice with mitochondrial diabetes. Nat Genet 2000;26:336–340
4. Supale S, Li N, Brun T, Maechler P. Mitochondrial dysfunction in pancreatic β cells. Trends Endocrinol Metab 2012;23:477–487
5. Molina AJ, Wikstrom JD, Stiles L, et al. Mitochondrial networking protects beta-cells from nutrient-induced apoptosis. Diabetes 2009;58:2303–2315
6. Park KS, Wiederkehr A, Kirkpatrick C, et al. Selective actions of mitochondrial fission/fusion genes on metabolism-secretion coupling in insulin-releasing cells. J Biol Chem 2008;283:33347–33356
7. Twig G, Elorza A, Molina AJ, et al. Fission and selective fusion govern mitochondrial segregation and elimination by autophagy. EMBO J 2008;27: 433–446
8. Anello M, Lupi R, Spampinato D, et al. Functional and morphological alterations of mitochondria in pancreatic beta cells from type 2 diabetic patients. Diabetologia 2005;48:282–289
9. Zhang Z, Wakabayashi N, Wakabayashi J, et al. The dynamin-related GTPase Opa1 is required for glucose-stimulated ATP production in pancreatic beta cells. Mol Biol Cell 2011;22:2235–2245
10. Coates PJ, Nenutil R, McGregor A, et al. Mammalian prohibitin proteins respond to mitochondrial stress and decrease during cellular senescence. Exp Cell Res 2001;265:262–273

11. Fusaro G, Dasgupta P, Rastogi S, Joshi B, Chellappan S. Prohibitin induces the transcriptional activity of p53 and is exported from the nucleus upon apoptotic signaling. J Biol Chem 2003;278:47853–47861
12. Nijtmans LG, de Jong L, Artal Sanz M, et al. Prohibitins act as a membrane-bound chaperone for the stabilization of mitochondrial proteins. EMBO J 2000;19:2444–2451
13. Terashima M, Kim KM, Adachi T, et al. The IgM antigen receptor of B lymphocytes is associated with prohibitin and a prohibitin-related protein. EMBO J 1994;13:3782–3792
14. Kolonin MG, Saha PK, Chan L, Pasqualini R, Arap W. Reversal of obesity by targeted ablation of adipose tissue. Nat Med 2004;10:625–632
15. Theiss AL, Vijay-Kumar M, Obertone TS, et al. Prohibitin is a novel regulator of antioxidant response that attenuates colonic inflammation in mice. Gastroenterology 2009;137:199–208, 208.e191–196
16. Merkwirth C, Langer T. Prohibitin function within mitochondria: essential roles for cell proliferation and cristae morphogenesis. Biochim Biophys Acta 2009;1793:27–32
17. Schleicher M, Shepherd BR, Suarez Y, et al. Prohibitin-1 maintains the angiogenic capacity of endothelial cells by regulating mitochondrial function and senescence. J Cell Biol 2008;180:101–112
18. Merkwirth C, Dargazanli S, Tatsuta T, et al. Prohibitins control cell proliferation and apoptosis by regulating OPA1-dependent cristae morphogenesis in mitochondria. Genes Dev 2008;22:476–488
19. Herrera PL. Adult insulin- and glucagon-producing cells differentiate from two independent cell lineages. Development 2000;127:2317–2322
20. American Diabetes Association. Standards of medical care in diabetes—2013. Diabetes Care 2013;36(Suppl. 1):S11–S66
21. Casimir M, de Andrade PB, Gjinovci A, Montani JP, Maechler P, Dulloo AG. A role for pancreatic beta-cell secretory hyperresponsiveness in catch-up growth hyperinsulinemia: Relevance to thrifty catch-up fat phenotype and risks for type 2 diabetes. Nutr Metab (Lond) 2011;8:2
22. Poy MN, Hausser J, Trajkovski M, et al. miR-375 maintains normal pancreatic alpha- and beta-cell mass. Proc Natl Acad Sci USA 2009;106:5813–5818
23. Carobbio S, Frigerio F, Rubi B, et al. Deletion of glutamate dehydrogenase in beta-cells abolishes part of the insulin secretory response not required for glucose homeostasis. J Biol Chem 2009;284:921–929
24. Carobbio S, Ishihara H, Fernandez-Pascual S, Bartley C, Martin-Del-Rio R, Maechler P. Insulin secretion profiles are modified by overexpression of glutamate dehydrogenase in pancreatic islets. Diabetologia 2004;47:266–276
25. Casimir M, Lasorsa FM, Rubi B, et al. Mitochondrial glutamate carrier GC1 as a newly identified player in the control of glucose-stimulated insulin secretion. J Biol Chem 2009;284:25004–25014
26. Li N, Li B, Brun T, et al. NADPH oxidase NOX2 defines a new antagonistic role for reactive oxygen species and cAMP/PKA in the regulation of insulin secretion. Diabetes 2012;61:2842–2850
27. Postic C, Shiota M, Niswender KD, et al. Dual roles for glucokinase in glucose homeostasis as determined by liver and pancreatic beta cell-specific gene knock-outs using Cre recombinase. J Biol Chem 1999;274:305–315
28. Wicksteed B, Brissova M, Yan W, et al. Conditional gene targeting in mouse pancreatic β-cells: analysis of ectopic Cre transgene expression in the brain. Diabetes 2010;59:3090–3098
29. Merkwirth C, Martinelli P, Korwitz A, et al. Loss of prohibitin membrane scaffolds impairs mitochondrial architecture and leads to tau hyperphosphorylation and neurodegeneration. PLoS Genet 2012;8:e1003021
30. de Andrade PB, Rubi B, Frigerio F, van den Ouweland JM, Maassen JA, Maechler P. Diabetes-associated mitochondrial DNA mutation A3243G impairs cellular metabolic pathways necessary for beta cell function. Diabetologia 2006;49:1816–1826
31. Ristow M, Mulder H, Pomplun D, et al. Frataxin deficiency in pancreatic islets causes diabetes due to loss of beta cell mass. J Clin Invest 2003;112:527–534
32. Wang MY, Chen L, Clark GO, et al. Leptin therapy in insulin-deficient type I diabetes. Proc Natl Acad Sci USA 2010;107:4813–4819
33. Mühlenhoff U, Richhardt N, Ristow M, Kispal G, Lill R. The yeast frataxin homolog Yfh1p plays a specific role in the maturation of cellular Fe/S proteins. Hum Mol Genet 2002;11:2025–2036
34. Bindokas VP, Kuznetsov A, Sreenan S, Polonsky KS, Roe MW, Philipson LH. Visualizing superoxide production in normal and diabetic rat islets of Langerhans. J Biol Chem 2003;278:9796–9801
35. Higa M, Zhou YT, Ravazzola M, Baetens D, Orci L, Unger RH. Troglitazone prevents mitochondrial alterations, beta cell destruction, and diabetes in obese prediabetic rats. Proc Natl Acad Sci USA 1999;96:11513–11518
36. Matsumoto S, Okitsu T, Iwanaga Y, et al. Insulin independence after living-donor distal pancreatectomy and islet allotransplantation. Lancet 2005;365:1642–1644
37. Meier JJ, Breuer TG, Bonadonna RC, et al. Pancreatic diabetes manifests when beta cell area declines by approximately 65% in humans. Diabetologia 2012;55:1346–1354
38. Unger RH, Cherrington AD. Glucagonocentric restructuring of diabetes: a pathophysiologic and therapeutic makeover. J Clin Invest 2012;122:4–12